Polarized neutron diffraction using a novel high- T c superconducting magnet on the single-crystal diffractometer POLI at MLZ

Article *in* Journal of Applied Crystallography · February 2018

DOI: 10.1107/S160057671800078X

CITATIONS
3

READS
39

4 authors, including:

Henrik Thoma
Forschungszentrum Jülich
6 PUBLICATIONS **10** CITATIONS
SEE PROFILE

V. Hutanu
RWTH Aachen University
73 PUBLICATIONS **254** CITATIONS
SEE PROFILE

JOURNAL OF APPLIED CRYSTALLOGRAPHY
ISSN 1600-5767

Polarized neutron diffraction using a novel high-T_c superconducting magnet on the single-crystal diffractometer POLI at MLZ[1]

Henrik Thoma,[a,b]* Wolfgang Luberstetter,[a,b] Jürgen Peters[c] and Vladimir Hutanu[a,b]*

[a]Institut für Kristallographie RWTH Aachen, Jägerstrasse 17–19, 52056 Aachen, Germany, [b]Jülich Centre for Neutron Science JCNS at MLZ, Lichtenbergstrasse 1, 85748 Garching, Germany, and [c]Forschungs-Neutronenquelle Heinz Maier-Leibnitz (FRM II), Lichtenbergstrasse 1, 85748 Garching, Germany. *Correspondence e-mail: henrik.thoma@frm2.tum.de, vladimir.hutanu@frm2.tum.de

Received 18 May 2017
Accepted 12 January 2018

Edited by G. J. McIntyre, Australian Centre for Neutron Scattering, Australia

[1] This article will form part of a virtual special issue on advanced neutron scattering instrumentation, marking the 50th anniversary of the journal.

Keywords: flipping ratio; polarized neutron diffraction; POLI single-crystal diffractometer for hot neutrons; ^{3}He spin-filter polarizers; high-T_c superconducting magnets.

Supporting information: this article has supporting information at journals.iucr.org/j

The polarized single-crystal diffractometer POLI is the first neutron scattering instrument routinely using ^{3}He spin filters both to produce and to analyse neutron polarization. The instrument, with a non-magnetic goniometer, was designed to perform two types of polarized neutron diffraction experiment: spherical neutron polarimetry, also known as full three-dimensional polarization analysis in zero magnetic field, and classical polarized neutron diffraction, also called the flipping-ratio (FR) method, in high applied magnetic fields. Reported here is the implementation of the FR setup for short-wavelength neutrons on POLI using a new high-T_c superconducting magnet with a maximal field of 2.2 T. The complete setup consists of a ^{3}He polarizer, a nutator, a Mezei-type flipper, guide fields and dedicated pole pieces, together with the magnet. Each component, as well as the whole setup, was numerically simulated, optimized, built and finally successfully tested under real experimental conditions on POLI. The measured polarized neutron spin transport efficiency is about 99% at different wavelengths, *e.g.* as short as 0.7 Å, and up to the maximal available field of the magnet. No further depolarization of the ^{3}He cells due to stray fields of the magnet occurs. The additional use of the available ^{3}He analyser allows uniaxial polarization analysis experiments in fields up to 1.2 T. The results of the first experiment on the field-dependent distribution of the trigonal antiferromagnetic domains in haematite (α-Fe_2O_3) are presented and compared with the literature data.

1. Introduction

Polarized neutron diffraction (PND) is a powerful method for investigating magnetic structures. It gives unique access to contributions from nuclear and magnetic scattering, their interference terms, and their magnetic chirality, and permits a distinction to be made between them. In contrast with non-polarized neutron diffraction, where the scattered intensity depends on the square of the magnetic structure factor, PND has a linear nuclear–magnetic interference term as part of the scattered intensity. This increases the precision in the determination of the ordered magnetic moment by at least one order of magnitude. In the classical flipping-ratio (FR) method, the sample is situated in a strong magnetic field. For each Bragg reflection, two scattered cross sections are measured for the two antiparallel oriented directions of the incoming neutron polarization, and the ratio between them is built. FR measurements are used for the refinement of magnetization density distribution maps (Deutsch *et al.*, 2014;

Brown *et al.*, 1979) and the determination of local anisotropy in the magnetic susceptibility at the unit-cell level (Gukasov & Brown, 2002). PND is also used for the high-quality determination of magnetic form factors (Lebech *et al.*, 1979; Wilkinson *et al.*, 1989), to untangle complex (*e.g.* chiral) magnetic structures and to follow the movement of magnetic domains (Nathans *et al.*, 1964). Born in the late 1950s (Nathans *et al.*, 1959) and developed over subsequent decades by small groups of devoted experts, PND is nowadays a widespread, well established and recognized technique to answer difficult scientific questions about the detailed magnetic ordering in topical materials, often intractable with other methods. This has become possible because of sustained instrumental improvement and development, especially in the past two decades. Dedicated instruments have been developed, like D3 and D23 at the ILL (Institut Laue-Langevin, Grenoble, France) or 5C1 (VIP) and 6T2 at the LLB (Laboratoire Léon Brillouin, Gif sur Yvette, France), as well as other instruments at different neutron scattering facilities all over the world, and they provide this type of experiment to a broad user community (Lelièvre-Berna *et al.*, 2005; Ressouche, 2005; Gukasov *et al.*, 2007, 2013). All of them use specially designed superconducting split-coil magnets cooled by a liquid-He bath for inducing sample magnetization.

In those magnets, an asymmetric field geometry is realized in order to assure an adiabatic transition for the neutron polarization between the opposite directed main field inside and the fringe field outside the magnet. If this transition is not adiabatic, and thus the magnetic field rotation is similar to or faster than the neutron Larmor frequency, the neutrons will depolarize. In the case of an asymmetric magnet, its fringe field also serves as guide field for the incoming neutrons.

Usually, the 111 Bragg reflection from a Heusler crystal monochromator is used on polarized diffractometers to produce a monochromatic polarized neutron beam. But, Heusler polarizers have a reduced reflectivity and poorer resolution for hot neutrons than for thermal neutrons, and a significant $\lambda/2$ contamination occurs in the incoming beam. However, hot neutrons are indispensable owing to their smaller absorption in magnetic studies of rare earth compounds and their wider Q-space access for precise form-factor determinations. Therefore, Lelièvre-Berna & Tasset (1999) proposed separating the monochromator from the polarizer by using, for example, a non-polarized focused Cu crystal monochromator in combination with a polarized ^{3}He spin filter cell (SFC). According to their calculations, it is possible to double the useful polarized neutron flux on the sample by optimizing both the flux from the non-polarized monochromator and the figure of merit of the SFC. Considering also the advantages of ^{3}He polarization technology for other neutron scattering techniques, like wide-angle polarization analysis in spectroscopy or small-angle neutron scattering, a real boost in the development and spread of the ^{3}He neutron polarization technique happened in the past decade. Today, ^{3}He SFCs are used as a standard method to analyse neutron polarization in Europe, USA, Japan and Australia. However, one of the drawbacks of this polarization method is that the SFCs should be hosted inside a very homogeneous magnetic field with a relative field gradient of the order of 10^{-4} cm^{-1}. This condition is difficult to maintain if the polarization device is situated in the vicinity of a strong superconducting magnet, because its strong and inhomogeneous fringe fields disturb the holding field of the SFC. To use the advantages of polarized ^{3}He spin filters on one hand and a high magnetic field at the sample position on the other, two different approaches are applied at different facilities. In the first approach, one tries to create new and better shielded magnetostatic cavities, for instance using superconducting Meissner shields (Dreyer *et al.*, 2000; Lelièvre-Berna *et al.*, 2010), which work with the available classical split-coil magnets at, for example, the ILL. The second approach is to develop new actively shielded magnets which provide significant smaller stray fields [typically at the level of 50 Oe (1 Oe = $100/4\pi$ A m^{-1}) at a distance of 1 m from the centre] (Oak Ridge Magnet Systems, https://neutrons.ornl.gov/sample/list/magnet-systems), for example at the Spallation Neutron Source (SNS, Oak Ridge, Tennesse, USA). Both these concepts use liquid-He-cooled superconducting materials, either to create or to screen the magnetic field or even both in combination.

At the Maier-Leibnitz Zentrum (MLZ) in Germany the new polarized single-crystal diffractometer POLI (polarization investigator) has been successfully developed and built over the past few years (Hutanu *et al.*, 2007; Hutanu, Meven *et al.*, 2009). POLI is the first instrument routinely using ^{3}He SFCs both to produce and to analyse neutron polarization (Hutanu *et al.*, 2011) in combination with double-focusing non-polarized monochromators (Hutanu, 2015). The spherical neutron polarimetry (SNP) setup using the third-generation polarimeter device Cryopad (Hutanu *et al.*, 2016) has been implemented on POLI as an initial experimental technique. However, with its non-magnetic sample table and goniometer, POLI was designed to support large and heavy sample environments like superconducting magnets in order to perform FR measurements as well. In the present report, we describe the new PND setup using a new high-T_c superconducting magnet which does not require any cryogen liquids, and therefore needs no maintenance related to their refilling and/or recovery. The new magnet described in the next section has a symmetric field with a maximal magnitude of 2.2 T and was purchased by MLZ as a standard all-round sample environment device suitable for different purposes. For the new PND setup on POLI, the ^{3}He polarizer and analyser available from the SNP setup are used. Using the advantages of the magnet's design, a novel approach in the guiding of the neutron polarization over the stray field and detailed numerical simulations of the whole setup, it was possible to realize a robust, simple, user friendly and relatively cheap setup for PND with short-wavelength neutrons on POLI. The high performance of the new setup is proven in the initial measurements. Two new PND methods using a magnetic field, namely FR and uniaxial polarization analysis (PA), are thus now available for users of POLI.

2. HTS magnet

A new compact magnet for neutron scattering experiments using high-T_c superconducting materials for high magnetic flux densities and cryogen-free operation has been produced by the HTS-110 company in New Zealand (http://www.hts-110.com/). A picture of the magnet, without the control electronics and He compressor, is shown in Fig. 1(*a*). The design of the magnet was the result of a complex optimization process of many parameters. The most important parameters specified by the MLZ as customer were the minimal size and weight of the magnet for a main field strength of 2 T and the maximum available angular access for the incoming and scattered beams.

With the magnet operating in the vertical position as shown in Fig. 1(*a*) (*z* axis vertical), the incoming neutron beam can reach the sample position in the centre of the magnet over the two large orifices shown at the right-back side and left-back side in the picture of the magnet. Both orifices have an angular opening of ±20°, permitting tilting and rotation of the magnet relative to the horizontal beam. The beam scattered from the sample has a horizontal access from −20 to 110° relative to the incoming beam and can be used in a right-handed or left-handed direction, depending on the incoming orifice used. Owing to this large horizontal access, the vertical positioning of the magnet makes diffraction experiments with large scattering angles possible. The vertical access of the scattered beam is also conical with an opening angle of ±20°. It permits either access to out-of-plane Bragg reflections for the investigation of single-crystal samples or the use of large two-dimensional detectors for powder diffraction. If the magnet is turned into the horizontal position with the *x* axis vertical, the field can be directed either along or perpendicular to the neutron beam in the plane (horizontal field geometry). This orientation gives access to three ±20° windows for the scattered beam. Although this could be used for some partial diffraction patterns, it is mostly interesting for small-angle neutron scattering (SANS) experiments. The large central room-temperature bore of 80 mm diameter allows the introduction of additional sample environment devices, such as cryo-furnaces, pressure cells *etc.*, into the field region of the magnet. This facilitates the neutron study of the physical properties of a sample dependent on different external parameters like temperature and magnetic field simultaneously. Such parametric studies are desired for the determination of magnetic phase diagrams or phase transitions.

The field at the sample position is directed along the *z* axis (*cf.* Fig. 1*a*) with a maximum strength of 2.2 T. Both field polarities are available. The coils, the iron yoke and consequently the magnetic field have a symmetric geometry with respect to the centre of the magnet and the equatorial *xy* plane; thus, the magnet was not designed at the outset for use with polarized neutrons. The distribution of the *z* component of the magnetic field at the maximal operating current along the *x* and *z* axes, respectively, is shown in Fig. 1(*b*). The black dashed curve denotes the absolute value of the main field strength as a function of distance from the magnet's centre. It decreases rapidly and reaches the reversal point, also called the zero-field node, at a distance of 151 mm from the centre. This point is only 15 mm away from the outer surface of the magnet's yoke body. The red dot-dashed curve denotes the absolute strength of the fringe field. It is easy to observe that the value of the fringe field at a distance of 1 m from the magnet's centre along the *x* axis is about 10 Oe for the maximal central field of 2.2 T. Having reduced stray fields of less than 15 Oe at a distance of 1 m from the sample was another request of the MLZ. In some new magnets for neutron scattering [*e.g.* MLZ Magnets (http://mlz-garching.de/englisch/instruments-und-labs/sample-environment/magnetic-fields.html) or Oak Ridge Magnet Systems (https://neutrons.ornl.gov/sample/list/magnet-systems)] this request is realized by adding additional coils situated further away from the centre and poled in the opposite direction relative to the main field, in order to compensate the fringe fields (actively shielded magnets). These have the disadvantage that the main field is also reduced and the size of the magnet increases. But since the magnet's size and field strength were the primary optimization parameters for the HTS magnet, passive shielding is a more promising approach in this case. It was realized using a massive and compact yoke of a soft magnetic material, surrounding the magnet and connecting the coils in order to concentrate and shortcut as much as possible of the fringe fields. The yoke's design is a compromise between the requests for a reduced fringe field and a maximal available angular access to the magnet's centre. In fact, the fringe field can be further decreased on a neutron scattering instrument by

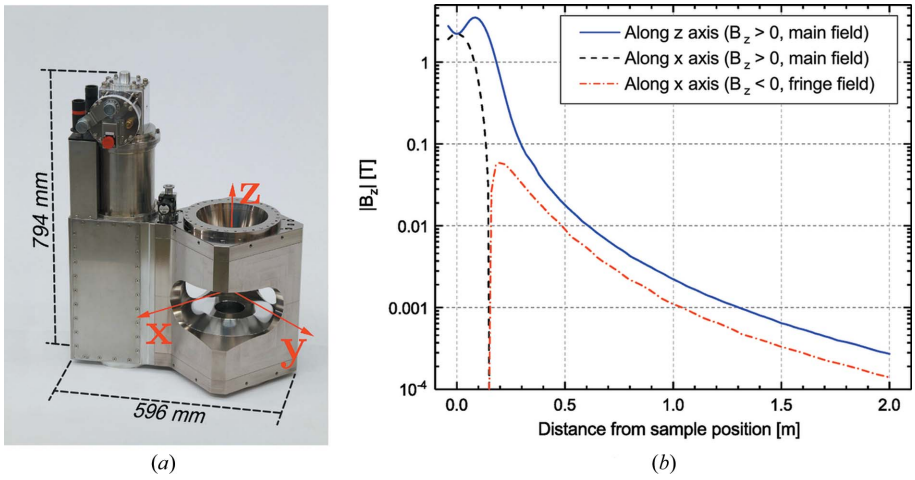

(*a*) (*b*)

Figure 1
(*a*) Photograph of the new MLZ HTS 2.2 T magnet as delivered, and the axis conventions used in the text. (*b*) Distribution of the *z* component of the magnetic field along the *x* and *z* axes at a maximal field strength of 2.2 T in the centre. The field reversal point is around 151 mm away from the sample position along the *x* axis.

closing access windows not used for the experiment with additional iron plates or plugs. The iron yoke gives the magnet a robust and compact monolithic form for an easy handling and installation on the beamline.

More technical details of the new HTS magnet can be found in the supporting information. For information on the development of high-T_c superconducting magnets at the HTS-110 company, we direct the interested reader to the work of Pooke *et al.* (2016).

3. HTS magnet on POLI

The single-crystal diffractometer POLI with a normal beam geometry has a maximal in-plane scattering angle γ of 130°. The scattered beam direction is to the left relative to the incoming beam (Hutanu, 2015). The measurement of out-of-plane reflections is possible using lifting mechanics for a single-tube neutron detector. Using this mechanism, the detector can access angles ν from −5 to 30° below and above the horizontal plane, respectively. Since the HTS magnet's large horizontal and vertical angular access fits well with the available solid-angle range at POLI, it can be efficiently used for single-crystal diffraction experiments in a magnetic field.

The compact and adaptive design of the HTS magnet allows its easy implementation on neutron instruments. Only a few adjustments were necessary to mount it on the sample table of POLI and use it for non-polarized neutron diffraction in a magnetic field (Hering *et al.*, 2017). On POLI, samples are usually studied at different temperatures, and the sample temperature is only limited by the performance of the cryostat used. Using an adapted MLZ-type closed-cycle refrigerator cryostat CCR5 in the HTS magnet, eventually in combination with dedicated low-temperature inserts, sample temperatures between 90 mK and 500 K are currently possible in a magnetic field on POLI. Moreover, the magnet has enough space to hold a pressure cell inside to apply pressure along any direction. The first user experiments on combined pressure–field dependence measurements using a non-polarized beam have been successfully performed on POLI (Pramanick *et al.*, 2016).

Initially, the HTS magnet with its symmetric field geometry was not designed for use with polarized neutrons. Thus, its implementation for FR measurements on POLI requires the solving of two main difficulties: First, the influence of the stray field on the performance of the ^{3}He polarizer and analyser must be avoided, and second, the zero-field node must be removed from the beam path in order not to disturb the polarization of the incoming beam. Because the stray field strength decays as the square of the distance from the centre, the first issue could in principle be easily overcome simply by increasing the distance between the magnet and the ^{3}He polarizer. However, on POLI the available experimental space is very limited. Therefore, a compromise between the maximal available distance of less than 1 m and proper shielding of the SFC is the only solution. We used a digital model, described in more detail in the next section, to optimize the distance between the magnet and the polarizer and to estimate the possible field influence on the position of the SFC. The result showed that, because of the rather small fringe field strength outside the yoke (*cf.* Fig. 1*b*) and the 2 mm thick μ-metal shielding of the SFC in the polarizer cavity, no significant depolarization of the SFC inside the polarizer situated 1 m away from magnet is expected. Fig. 2 shows the measured time-dependent transmission of the SFC in the polarizer for a non-polarized beam, together with the field history in the magnet for a particular experiment (Pramanick *et al.*, 2016), as an example. As shown in the figure, multiple ramping of the magnet between maximal and minimal field does not influence the typical cell performance at all.

For loss-free guiding of neutron polarization, it is necessary to keep the rotation frequency of the magnetic guide field significantly lower than the neutron Larmor frequency. For the general case of a field with constant magnitude B (in T) which reverses its direction over a length S (in m), the depolarization rate ΔP can be estimated by the following relation:

$$\Delta P \leq \frac{2}{1+E^2}, \qquad (1)$$

with $E = 15\,000\,BS\lambda$, where λ is the wavelength of the neutrons (in Å). To keep the depolarization less than 1%, $E \geq 14$ must be provided. This is typically realized by shifting the zero-field node above or below the path of the incoming neutrons in order to increase the length S and provide an adiabatic neutron transition condition. This leads to an asymmetric field distribution in the equatorial plane of the magnet.

For the symmetrical HTS magnet, the zero-field node is situated exactly in the horizontal plane close to the outer surface of the yoke. In order to suppress it, we introduced through the large openings of the magnet two iron plates

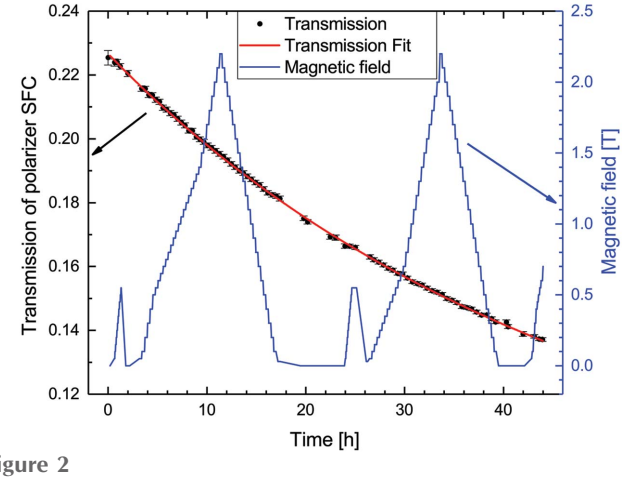

Figure 2
Time dependence of the total neutron transmission for a non-polarized 20 mm diameter beam in a typical ^{3}He polarizer SFC (6 cm diameter and 13 cm long) at 2.34 bar (2.34×10^5 Pa) pressure and a wavelength of 1.15 Å on POLI, registered during the field variation in the magnet for a particular experiment (Pramanick *et al.*, 2016). The gaps in the transmission measurement correspond to time frames with no scan data taken (*e.g.* during cooling or heating of the sample). The values for the starting polarization $P_0 = 73.39\,(2)\%$ and for the time relaxation constant $T_1 = 127.0\,(2)$ h result from the data fit and are comparable to those usually obtained in SNP measurements.

inside the yoke and connected them to the magnet's poles close to its centre, without touching the yoke. In this way, the main field direction can be extracted to the outside of the magnet and directly coupled to a guide field. For the first time, the guide field is directed not along the stray field as is usual for an asymmetric field geometry but along the main field direction. The ends of the plates were coupled to the magnetic poles of the nutators, available from POLI's SNP setup (Hutanu *et al.*, 2016). Initial test experiments showed the feasibility of this approach. The main field strength inside the magnet did not change significantly and it was even possible to flip the incoming neutron spin by switching the direction of the current in the nutator coils. However, the direct coupling between the main field direction and the opposite field in the nutator for flipping was slightly adiabatic and the flipping efficiency correspondingly poor. As result, a fixed guide field between the polarizer and the magnet, including iron pole pieces of optimized form and size, and an additional flipper were developed.

4. Development of guide field and Mezei spin flipper

Starting from the real geometry of the coils and the magnetic yoke, the HTS magnet was modelled using the COMSOL *Multiphysics* software package (https://www.comsol.com/). By tuning the material properties of the yoke in the model, a very good agreement between the measured and COMSOL-simulated main and fringe field values were achieved for different currents (see Fig. S1 in the supporting information). In the next step, a first draft of the guiding field plates was set up and their performance simulated in the field of the HTS magnet. In an iterative process, this draft was optimized regarding several aspects including the length, shape and thickness of the pole pieces. Using COMSOL's *LiveLink for MATLAB* (https://www.comsol.com/livelink-for-matlab), the simulated field map was read out directly and forwarded to a bespoke C program, which calculated the expected polarization losses for the complete beam profile based on the simulated field data. Finally, the average polarization transport efficiency over this profile served as reference for the comparison between the different drafts. Since the whole simulation procedure was fully controlled by a *MATLAB* script and the quality of each draft could be broken down into a single parameter, namely the spin transport efficiency, the optimization process of individual components could be almost completely automated. As an example, a comparison of four different shapes of the pole pieces is shown in Fig. S2 in the supporting information. The final design of the guide field segment attached to the magnet, together with other components, is shown in Fig. 3(*a*). The guiding of the main field out of the magnet, using the pole pieces inserted close to the centre of the magnet shown in orange [position 7 in Fig. 3(*a*)], is clearly visible in Fig. 3(*b*). The field-reversal node from Fig. 1(*b*), discussed in the previous section, does not occur in the beam path. It is remarkable that the guide field originates only from the main field of the magnet, with no additional permanent magnets or coils being used. However, to withstand the fringe field at maximal magnet power, the pole pieces of the guide field are shielded by a cylindrical 5 mm thick iron envelope, also optimized using the described digital model [shown in dark grey at position 7 in Fig. 3(*a*)]. Connected to the shielding, an iron nose going into the magnet was added to bridge the fringe fields in the immediate vicinity of the input window of the magnet [clearly seen in Fig. 3(*b*)].

As discussed in the previous section, a non-adiabatic spin transition between the polarizer and the magnetic guide field (in our case the main field in the magnet) needs to be provided for a spin flip. For hot neutrons, a cryoflipper, exploiting the superconducting Meissner effect, is usually used (Tasset, 1989). This flipper type has the advantage of being very compact in the beam path and rather robust with regard to stray fields of the magnet. On the downside, the flipper must be cooled continuously to maintain its superconducting state, which is costly and needs additional maintenance. Even in the recently proposed cryoflipper prototypes using the high-T_c material YBCO instead of a classical Nb sheet (Parnell *et al.*, 2013), a dedicated cold head with associated He compressor is necessary, although there is no need for cooling down to liquid-He temperatures. Having two dedicated compressors already, the first for the magnet and second for the cryostat inside the magnet, and very limited space in the experimental field as well as a limited budget, we searched for an alternative solution. Babcock *et al.* (2007) proposed a radio frequency

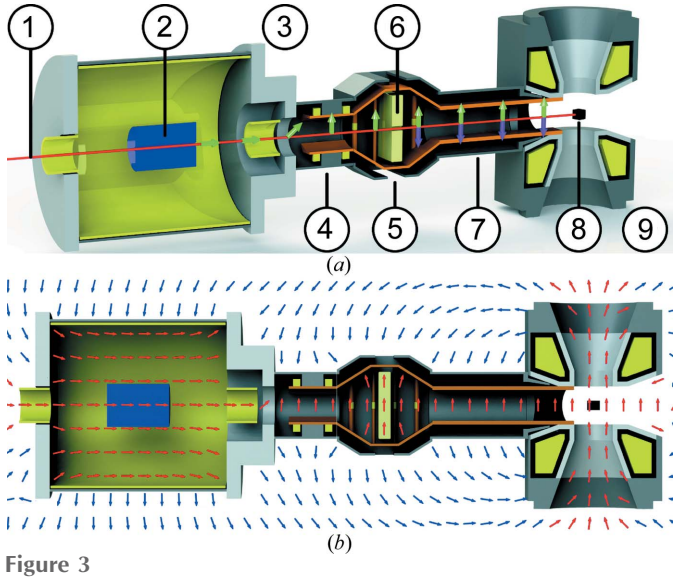

Figure 3
Setup components of POLI, with coils shown in yellow, guiding field pole pieces in orange, and magnetic yoke and shielding parts in dark grey. (*a*) Overview of the setup components: (1) the non-polarized incoming monochromatic neutron beam; (2) the ^{3}He SFC inside (3) the magnetostatic cavity, with main and two correction coils; (4) the nutator, which turns the spin perpendicular to the beam direction; (5) the shielded guide field produced by permanent magnets around (6) the Mezei flipper; (7) the shielded guide field between flipper and magnet with pole pieces going inside the magnet (orange) and the iron nose (dark grey); (8) the sample; and (9) the HTS magnet. The polarization direction of the neutrons is shown as green arrows. The purple arrows correspond to the polarization with the activated spin flipper. (*b*) The magnetic field distribution inside the polarizer, guide field and magnet. The direction of the main field is shown in red and the fringe field in blue.

(RF) flipper for short neutron wavelengths and an adiabatic fast passage (AFP) flipper for ^{3}He in the polarizer. The first one requires about 50–70 cm space in the beam path and is thus too large for POLI. This drawback is absolutely absent for the AFP flipper integrated into the polarizer magnetostatic chamber. However, each flip of the polarized ^{3}He gas spin leads to a slight relaxation of the polarization efficiency of the SFC. Taking into account long FR measurements (over several days) on POLI with frequent spin flips (1 Hz), even the lowest reported loss per flip rate for such a flipper in the literature of the order of 10^{-5}–10^{-4} will lead to a significant additional depolarization of the incoming beam. In contrast, a Mezei-type double-coil flipper (Mezei, 1972) is cheap in realization and operation, has a simple and robust design, and is quite compact in the beam direction. The typical disadvantages of Mezei flippers are a limited current in the coils, their dependence on external fringe fields and some beam attenuation occurring on the windings in the beam path. This last problem is not significant for hot neutrons. Measured on POLI at a wavelength of 0.9 Å, the attenuation of the counting rate caused by the introduction of the Mezei coil in the beam is about 1.4% and can be neglected. Keeping in mind that the fringe field of the new HTS magnet is significantly weaker than that for typical superconducting magnets, we chose a Mezei-type flipper to control the incoming neutron polarization in our setup. For the design of the new flipper, detailed numerical simulations were used to optimize for the large-cross-section and short-wavelength neutron beam, for the close vicinity (0.5 m) to the HTS magnet, for the new guide field segment with the guiding field opposite to the fringe field, and for the ^{3}He polarizer. The main criteria have been an efficient neutron spin flip for all available wavelengths on POLI from 0.55 to 1.15 Å and a maximum independence of the HTS magnet's main field, to minimize variations in the compensation coil current and guarantee a stable flipping efficiency. Finally, the strictly limited available space in the beam path has been considered. Technical details of the new Mezei flipper on POLI and the results of its calibration are presented in the supporting information. A high flipping efficiency at different wavelengths and all available fields in the magnet has been experimentally proven.

5. Instrumental options for polarized neutron diffraction in a magnetic field on POLI

Using the presented setup with the HTS magnet, two different instrumental options for PND in a magnetic field become available on POLI. Firstly, we discuss the setup for FR measurements, using only one SFC as polarizer and the lifting counter as detector. Polarization-dependent scattering cross sections on a large number of Bragg reflections can be measured, since the detector can reach out-of-plane peaks. For this kind of measurement, a good polarized neutron transport efficiency between the polarizer and the sample is mandatory. Fig. 4(*a*) shows a photograph of the FR setup. The non-polarized beam from a focused monochromator arrives from the right-hand side in the picture. It is polarized along the beam propagation direction by the SFC inside the polarizer cavity (1) [corresponding to positions 2 and 3 in Fig. 3(*a*)]. The nutator (2) [position 4 in Fig. 3(*a*)] turns the neutron polarization transverse to the beam propagation direction. The flipper (3) [positions 5 and 6 in Fig. 3(*a*)] controls the up/down polarization direction. The shielded guide field (4) [position 7 in Fig. 3(*a*)] is fixed on the magnet's yoke (5). The sample (6) is placed inside a CCR cryostat (7), inserted vertically and fixed on the top of the magnet. The scattered neutrons are counted by the lifting counter (8). No polarization losses were observed using this setup, up to the maximal available field of the magnet.

Adding an analyser and a second flipper for the scattered neutrons to the setup above permits the performing of uniaxial PA along the quantization axis of the main magnetic field. Such a setup, first used and described by Moon *et al.* (1969), allows the measurement of changes in neutron polarization through scattering and a distinction to be made between the nuclear and magnetic scattering contributions.

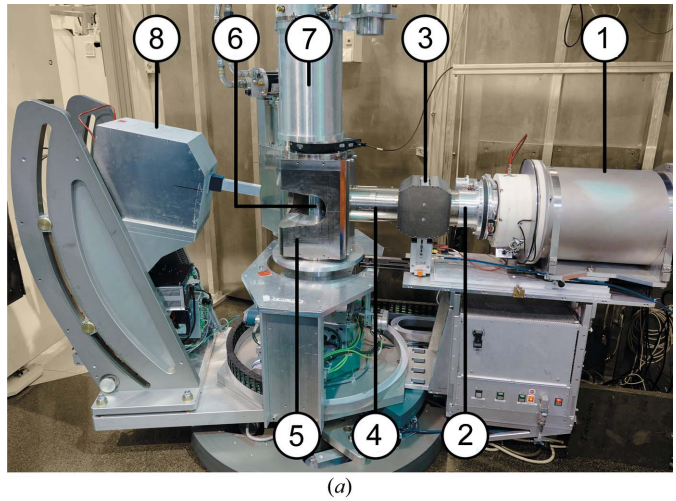

(*a*)

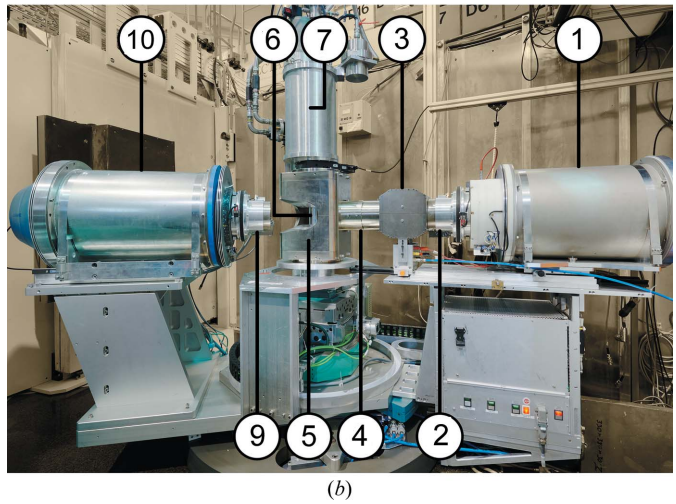

(*b*)

Figure 4
(*a*) The PND setup using the new HTS magnet and a lifting detector for FR measurements on POLI. (*b*) The PND setup using the new HTS magnet and the Decpol for uniaxial PA experiments on POLI. The notation of the numbered components is given in the main text.

On POLI, an SFC analyser with an integrated single counter, called Decpol (Hutanu, Meven *et al.*, 2009), is available as a standard device for performing SNP measurements (Hutanu *et al.*, 2016). As shown in the photograph of the resulting PA setup in Fig. 4(*b*), we used this Decpol (10) with a fixed second nutator (9) without any further changes, in combination with the HTS magnet, in order to prove the feasibility of the uniaxial PA in a magnetic field on POLI. In contrast with the previous method, a good polarized neutron transport efficiency is important for this type of measurement for the whole path between the polarizer and the detector, because the polarization is analysed after the scattering by the sample. Here, the studied Bragg reflections are limited to the horizontal scattering plane only. An almost-perfect transport efficiency could be confirmed using the Decpol for PA up to 1.2 T in the HTS magnet, without any additional effort. At higher fields in the magnet, the field of the second nutator of 120 Oe is not sufficient to suppress the zero-field node and, as a consequence, stray fields become dominant. Our tests with iron plates situated inside the magnet, similar to those on the primary side, demonstrated that it is possible to extend the polarization transmission efficiency easily, without losses, to at least 1.7 T. However, to make it available for the complete wide scattering angle range in the horizontal plane, an additional guide field for the scattered beam should be designed and built. This development was beyond the scope of the present report and can be addressed in the future, if uniaxial PA experiments in the field region between 1.2 and 2.2 T are requested on POLI.

6. Initial measurements

In a first measurement, the performance of the FR and PA setups described in §5 was tested using the new HTS magnet and ^{3}He SFC as well as other components. The currents in the flipping and compensation coils, respectively, of the Mezei flipper were calibrated for all fields in the magnet starting from 0.1 T up to 2.2 T in 0.1 T steps. The optimal flipper currents were applied for each discrete field in the following polarization measurements. More details about the flipper calibration are given in the supporting information.

6.1. Measurement of the spin transport efficiency

Using neutron polarization measurements on a purely nuclear Bragg reflection, direct access to the polarized neutron spin transmission efficiency of the setup is given. Since there is no magnetic contribution to the nuclear peak, the spin state is conserved during the scattering process. Thus, the polarization before and after the sample remains the same. In this case, the product of the polarizing and analysing efficiencies, $P_{\rm Pol}$ and $P_{\rm An}$, respectively, and the polarized neutron spin transport efficiency $P_{\rm t}$ of the setup, accounting for all setup-related losses and the flipping efficiency, is given by the typical relation for the asymmetry

$$P_{\rm Pol}P_{\rm An}P_{\rm t} = \frac{I^+ - I^-}{I^+ + I^-}, \qquad (2)$$

where I^+ and I^- are the counting rates obtained with deactivated and activated flippers, respectively. The PA setup option with the Decpol and the ^{3}He SFC analyser was used to prove the efficiency $P_{\rm t}$ in the low-field region. By measuring the transmission of a non-polarized neutron beam in each SFC, $P_{\rm Pol}$ and $P_{\rm An}$ can be determined precisely, for example using the formulae presented by Hutanu *et al.* (2011), where typical SFCs used on POLI are also described. Afterwards, using the experimentally determined asymmetry from equation (2), $P_{\rm t}$ can be easily calculated.

In our measurement, the nuclear 0018 reflection of a haematite (α-Fe_2O_3) single-crystal sample was used. The resulting $P_{\rm t}$ obtained from the asymmetry by normalizing for the efficiencies of the SFCs used is shown in Fig. 5 with circle symbols. A constant and high $P_{\rm t}$ value of 98–99% was observed for all fields from 0.1 to 1 T using the PA setup.

For the FR option with lifting counter, a Heusler (Cu_2MnAl) single-crystal sample situated in the magnet is used as analyser. In general, the resulting scattering intensity for a magnetic sample is polarization (P) dependent according to

$$\frac{{\rm d}\sigma}{{\rm d}\Omega} = \underbrace{NN^*}_{\rm nuclear} + \underbrace{\mathbf{M}_\perp\mathbf{M}_\perp^*}_{\rm magnetic} + P\left\{\underbrace{2\Re\left[\mathbf{M}^*_{(\perp,\parallel)}N\right]}_{\rm nucl.\,mag.\,interference} - \underbrace{i(\mathbf{M}_\perp \times \mathbf{M}_\perp^*)\hat{\mathbf{e}}_H}_{\rm chiral}\right\}, \qquad (3)$$

with $\mathbf{M}_\perp$ the magnetic contribution perpendicular to the scattering vector and N the nuclear one. $\mathbf{M}_\perp$ can be further subdivided into $\mathbf{M}_{(\perp,\parallel)}$ parallel to the external field with direction $\hat{\mathbf{e}}_H$ (Blume, 1963).

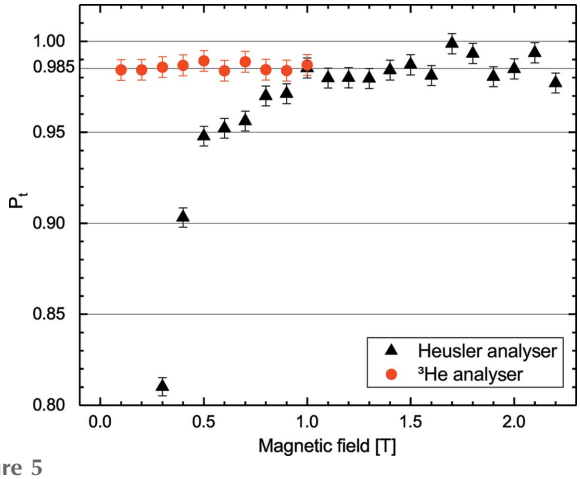

Figure 5
The polarized neutron spin transport efficiency $P_{\rm t}$ as a function of the main field in the magnet, obtained from asymmetry measurements with a wavelength of 0.7 Å. The circle symbols denote values obtained from equation (2) at a lower field using the PA setup with the SFC as analyser. The triangles show the values obtained from equation (5) using the FR setup with a Heusler crystal as analyser.

The Heusler crystal has no chiral contribution but is ferromagnetic. This leads to mixed nuclear–magnetic reflections. For the 111 reflection of the Heusler crystal, the sum of the pure magnetic and nuclear terms equals the negative interference term,

$$NN^*_{111} + \mathbf{M}_\perp \mathbf{M}^*_{\perp\,111} \simeq -2\Re\left[\mathbf{M}^*_{(\perp,\parallel)} N\right]_{111}. \quad (4)$$

Thus, almost no spin-up neutrons are scattered and the crystal can be used as an analyser. Note, however, that this is only valid for a single domain state. For multiple domains the interference term is reduced and the analysing efficiency decreases.

SF measurements on the 111 reflection of the Heusler crystal allow extraction of the neutron polarization at the sample position, reduced by the polarizing efficiency $P_{\rm Pol}$ of the SFC, the analysing efficiency of the Heusler crystal $P_{\rm Heusler}$ and the spin transport efficiency $P_{\rm t}$ as a function of the applied magnetic field. This product is again given by the relation for the asymmetry,

$$P_{\rm Heusler} P_{\rm Pol} P_{\rm t} = \frac{I^+ - I^-}{I^+ + I^-}. \quad (5)$$

Whereas $P_{\rm Pol}$ can be calculated as mentioned above, $P_{\rm Heusler}$ depends on the domain distribution of the Heusler crystal, and thus on the applied field, until its saturation above 1 T. By assuming $P_{\rm t}$ to be equal for the PA and FR setups in the low-field region, which is reasonable since the FR setup differs from the PA setup only in the shorter distance between the polarizer and analyser, the analysing efficiency of the Heusler crystal in saturation at 1 T can be extracted with a value of 95%. This agrees perfectly with the value given in the literature (*e.g.* Courtois, 1999).The resulting $P_{\rm t}$ value, calculated by normalizing the measured asymmetry for $P_{\rm Pol}$ and a constant $P_{\rm Heusler}$ of 95%, is shown in Fig. 5 by triangular symbols. It is easy to observe that high $P_{\rm t}$ values between 0.98 and 1 are obtained for the saturated Heusler crystal, and they are independent of the field in the magnet up to the maximal available value of 2.2 T.

Below the saturation field of about 1 T, the Heusler crystal has a multi-domain structure, leading to a reduced analysing efficiency $P_{\rm Heusler}$. Since $P_{\rm Heusler}$ was assumed to be constant, this results in a drop in the calculated $P_{\rm t}$ towards lower fields and reveals the field-dependent saturation behaviour which is typical for large Heusler crystals (Gukasov, 2017).

Combining both higher and lower field measurements, one can conclude that the setup offers a constant and high spin transport efficiency of about 98.5% over the full field range of the HTS magnet.

6.2. Measurement of a magnetic test sample

To test the performance of the PND setup with a real magnetic sample, the field dependence of the domain distribution ratio in a haematite (α-Fe_2O_3) single crystal was investigated. Hematite has a rhombohedral structure in space group $R\bar{3}c$ (No. 167, *International Tables for Crystallography*; Hahn *et al.*, 2010). In the temperature range between the Morin temperature of about 259 K and the Néel temperature of 955 K, it is antiferromagnetic with spins lying in the basal plane of the hexagonal setting (Hill *et al.*, 2008). In this room-temperature phase, haematite has 120° structural domains. Within each of these trigonal domains, two equivalent 180° antiferromagnetic domains exist (Nathans *et al.*, 1964). It is not possible to distinguish between them using non-polarized neutron diffraction or other methods. For our experiment, we used the uniaxial PA setup option with the SFC as polarizer and analyser.

If we consider the purely magnetic 003 Bragg reflection, the nuclear and nuclear–magnetic interference terms vanish while the scattering vector is normal to the basal plane. The sample is oriented with the external magnetic field in the basal plane. The directions of the magnetic field relative to the crystal axis and the trigonal domains are visualized in Fig. 6(*a*). For these conditions, the spin-flip and non-spin-flip scattering cross sections reduce to

$$\left(\frac{{\rm d}\sigma}{{\rm d}\Omega}\right)^{\pm\to\pm}_{(003)} = \mathbf{M}_{\parallel H}\mathbf{M}^*_{\parallel H} = \frac{3}{4}(d_2 + d_3)\mathbf{M}\mathbf{M}^*, \quad (6)$$

$$\left(\frac{{\rm d}\sigma}{{\rm d}\Omega}\right)^{\pm\to\mp}_{(003)} = \mathbf{M}_{\perp H}\mathbf{M}^*_{\perp H} = \left(d_1 + \frac{1}{4}d_2 + \frac{1}{4}d_3\right)\mathbf{M}\mathbf{M}^*. \quad (7)$$

If we assume domains d_2 and d_3 to be equally distributed, since they enclose the same angle with the magnetic field, the resulting polarization P of the neutrons is directly related to the domain population d_1 and should approach $d_1 = 1/3$ for low applied fields (*i.e.* equally distributed domains) and $d_1 = 1$ (mono-domain situation) for high applied fields, as expected for antiferromagnetic domains oriented perpendicular to the external field:

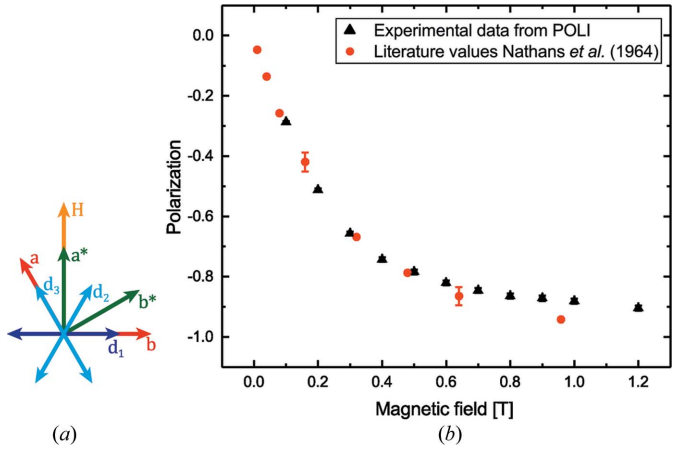

(*a*) (*b*)

Figure 6
(*a*) The orientation of the haematite single-crystal sample relative to the main field H in the HTS magnet on POLI. a, b and a^*, b^* are the direct and reciprocal-lattice vectors, respectively. The antiferromagnetic domains are labelled as d_1, d_2 and d_3. (*b*) Normalized scattered polarization from the purely magnetic 003 reflection, measured as a function of the applied magnetic field. The error bars are smaller than the symbols.

$$d_1 = \frac{1}{3}(1 - 2P). \quad (8)$$

The measured scattered polarization P as a function of the applied magnetic field in α-Fe_2O_3 at room temperature, corrected for the polarizing efficiency of the SFCs as polarizer and analyser using the procedure described by Hutanu and co-workers (Hutanu *et al.*, 2011; Hutanu, Janoschek *et al.*, 2009), is shown in Fig. 6(*b*). The result shows a fully depolarized beam at zero external field, denoting a perfect statistical distribution of the 120° domains in the studied sample. The population of the d_1 domain perpendicular to the applied field increases continuously with applied field strength. The saturation process starts at fields above 0.3 T, when the d_1 domain reaches about 2/3 of the sample volume. At fields above 0.6 T, the population of the d_1 domain increases slowly (almost linearly) with the field, not yet reaching the fully monodomain state at 1.2 T (volume ratio 0.94). Our results are compared with the literature data from Nathans *et al.* (1964), also shown in Fig. 6(*b*). It is easy to observe the almost-perfect agreement between the two measurements. Only for fields higher than 0.6 T was a small difference in the saturation behaviour observed. Since Nathans *et al.* (1964) reported a similar difference in the saturation of a natural and a synthetic haematite crystal, this effect might be attributed to an individual crystal effect. Moreover, even a very small misalignment between the field and the crystal lattice orientation can lead to a sizeable effect for the measured FR or polarization (and, respectively, for the non-monodomain situation). For example, during the experiment it was observed that a 2° tilting of the crystal relative to the perfect field alignment leads to a difference of about 0.04 (1) in the measured polarization.

7. Conclusions

A new magnet for neutron scattering using high-T_c superconducting materials which do not require liquid cryogens and providing a maximal field of 2.2 T has been successfully developed and built by the HTS-100 company in collaboration with the MLZ. The HTS magnet is very compact, relatively light, has large access angles to the sample position, and can be easily used for different types of neutron experiment like powder or single-crystal diffraction, SANS, spectroscopy *etc.* The HTS magnet was successfully implemented on the single-crystal neutron diffractometer POLI. Structural studies in magnetic fields up to 2.2 T at different temperatures and pressures are thus now available for POLI users. Through an innovative approach, this magnet was adopted for PND, using an existing ^{3}He polarizer together with a newly developed flipper and a special guide field segment, which is inserted into the magnet. This setup, carefully optimized by numerical simulations, provides almost loss-free passage of the neutron polarization though the instrument.

A polarization transport efficiency of about 99% could be measured using a short neutron wavelength of 0.7 Å. The setup works at all available wavelengths on POLI from 0.55 to 1.15 Å. No additional depolarization from the magnet's fringe field occurs in the ^{3}He SFC. Two polarized neutron diffraction options, namely FR measurement and uniaxial PA, were successfully tested and their performance demonstrated. Using the new polarized setup, the field dependence of the trigonal antiferromagnetic domain distrubution in haematite (α-Fe_2O_3) has been measured and compared with the earlier data from Nathans *et al.* (1964). A very good agreement between the POLI results and the literature data validates the quality of the new setup and opens the way for using it for precise magnetic investigations by the wider user community.

Acknowledgements

We are grateful to G. Brandl for support in setting up the control software for the new magnet on POLI.

Funding information

This work was supported by the German Ministry for Education and Research BMBF through project No. 05K13PA3. The POLI instrument is operated by RWTH Aachen/FZ Jülich (Jülich Aachen Research Alliance JARA).

References

Babcock, E., Petoukhov, A., Chastagnier, J., Jullien, D., Lelièvre-Berna, E., Andersen, K. H., Georgii, R., Masalovich, S., Boag, S., Frost, C. D. & Parnell, S. R. (2007). *Physica B*, **397**, 172–175.
Blume, M. (1963). *Phys. Rev.* **130**, 1670–1676.
Brown, P. J., Capiomont, A., Gillon, B. & Schweizer, J. (1979). *J. Magn. Magn. Mater.* **14**, 289–294.
Courtois, P. (1999). *Physica B*, **267–268**, 363–366.
Deutsch, M., Gillon, B., Claiser, N., Gillet, J.-M., Lecomte, C. & Souhassou, M. (2014). *IUCrJ*, **1**, 194–199.
Dreyer, J., Regnault, L. P., Bourgeat-Lami, E., Lelièvre-Berna, E., Pujol, S., Thomas, F., Thomas, M. & Tasset, F. (2000). *Nucl. Instrum. Methods Phys. Res. A*, **449**, 638–648.
Gukasov, A. (2017). Personal communication.
Gukasov, A. & Brown, P. J. (2002). *J. Phys. Condens. Matter*, **14**, 8831–8839.
Gukasov, A., Goujon, A., Meuriot, J., Person, C., Exil, G. & Koskas, G. (2007). *Physica B*, **397**, 131–134.
Gukasov, A., Rodrigues, S., Meuriot, J., Robillard, T., Sazonov, A., Gillon, B., Laverdunt, A., Prunes, F. & Coneggo, F. (2013). *Phys. Proc.* **42**, 150–153.
Aroyo, M. I. (2016). Editor. *International Tables for Crystallography*, Vol. A, *Space-Group Symmetry*, 2nd online ed. Chester: International Union of Crystallography.
Hering, P., Friese, K. & Voigt, J. (2017). MLZ Experimental Report No. 4141. Heinz Maier-Leibnitz Zentrum, Garching, Germany.
Hill, A. H., Jiao, F., Bruce, P. G., Harrison, A., Kockelmann, W. & Ritter, C. (2008). *Chem. Mater.* **20**, 4891–4899.
Hutanu, V. (2015). *J. Large-Scale Res. Facil.* **1**, A16.
Hutanu, V., Janoschek, M., Meven, M., Böni, P. & Heger, G. (2009). *Nucl. Instrum. Methods Phys. Res. A*, **612**, 155–160.
Hutanu, V., Luberstetter, W., Bourgeat-Lami, E., Meven, M., Sazonov, A., Steffen, A., Heger, G., Roth, G. & Lelièvre-Berna, E. (2016). *Rev. Sci. Instrum.* **87**, 105108.
Hutanu, V., Meven, M. & Heger, G. (2007). *Physica B*, **397**, 135–137.
Hutanu, V., Meven, M., Lelièvre-Berna, E. & Heger, G. (2009). *Physica B*, **404**, 2633–2636.
Hutanu, V., Meven, M., Masalovich, S., Heger, G. & Roth, G. (2011). *J. Phys. Conf. Ser.* **294**, 012012.

Lebech, B., Rainford, B. D., Brown, P. J. & Wedgwood, F. A. (1979). *J. Magn. Magn. Mater.* **14**, 298–300.
Lelièvre-Berna, E., Bourgeat-Lami, E., Gibert, Y., Kernavanois, N., Locatelli, J., Mary, T., Pastrello, G., Petukhov, A., Pujol, S. & Rouques, R. (2005). *Physica B*, **356**, 141–145.
Lelièvre-Berna, E. & Tasset, F. (1999). *Physica B*, **267–268**, 21–26.
Lelièvre-Berna, E., Wills, A. S. *et al.* (2010). *Meas. Sci. Technol.* **21**, 055106.
Mezei, F. (1972). *Z. Phys.* **255**, 146–160.
Moon, R. M., Riste, T. & Koehler, W. C. (1969). *Phys. Rev.* **181**, 920–931.
Nathans, R., Pickart, S. J., Alperin, H. A. & Brown, P. J. (1964). *Phys. Rev.* **136**, A1641–A1647.
Nathans, R., Shull, C. G., Shirane, G. & Andresen, A. (1959). *J. Phys. Chem. Solids*, **10**, 138–146.
Parnell, S., Washington, A. L., Kaiser, H., Li, F., Wang, T., Hamilton, W., Baxter, D. & Pynn, R. (2013). *Nucl. Instrum. Methods Phys. Res. A*, **722**, 20–23.
Pooke, D., Fee, M., Huang, T., Chamritski, V. & Christian, M. (2016). *Research, Fabrication and Applications of Bi-2223 HTS Wires*, ch. 3.15, pp. 379–402. Singapore: World Scientific.
Pramanick, A., Ke, Y. & Wang, X.-L. (2016). MLZ Experimental Report No. 4138. Heinz Maier-Leibnitz Zentrum, Garching, Germany.
Ressouche, E. (2005). *ILL Yellow Book*, 2005 ed., pp. 44–45. Institut Laue–Langevin, Grenoble, France.
Tasset, F. (1989). *Physica B*, **156–157**, 627–630.
Wilkinson, C., Keen, D. A., Brown, P. J. & Forsyth, J. B. (1989). *J. Phys. Condens. Matter*, **1**, 3833–3839.